# Dynamic Simulation of Variable Topology Tetrahedral Robot

Chun LI, Hong NIE, Jinbao CHEN

State Key Laboratory of Mechanics and Control of Mechanical Structures, Nanjing University of Aeronautics and Astronautics, Nanjing, 210016, China

***Abstract* — To improve the model accuracy of a variable topology tetrahedral robot, a method for constriction of the model based on boundary constraint RBF is proposed. Firstly, dynamic equations and their integral characteristics of the model are analyzed, with the model reduction method adopted to reduce order of the partially integrable model equation to two totally integrable sub-equations. Secondly, constraint conditions for boundary values of solution are used to obtain the penalty function, while the least square method is adopted to train the traditional RBF neural network to realize construction of the model of the variable topology tetrahedral robot. Finally, efficiency of the model is verified by experimental simulation.**

***Keywords - boundary constraint; rbf network; variable topology; tetrahedral robot***

## I. INTRODUCTION

The variable topology tetrahedral robot is a nonlinear system designed to reach the requirements of reducing weight and further reducing power consumption, decrease driving devices and achieve the system's number of input being less than the number of degree of freedom. A kinetic modular model established by a standard method cannot be applied to such a system which does not meet STLC determination conditions also, so there is a large amount of difficult calculation to solve inverse kinematics relationships. For high-order systems, calculations cannot be made by values, and positive and inverse solutions are directly worked out.

For the variable topology tetrahedral robot system, domestic and foreign scholars have conducted wide researches and made some achievements. A preliminary study is made on the integrable characteristic of the variable topology tetrahedral robot in Literature [], which provides basis and methods of calculation for kinetic relations between active and passive joints of the variable topology tetrahedral robot. The inverse solution of the variable topology tetrahedral robot system is worked out by use of the particle swarm optimization in Literature [] which, however, uses the method of which the rate of convergence is slower and does not optimize the method. Such intelligent algorithms as the genetic algorithm are applied to motion control of the plane variable topology tetrahedral robot system in Literature [], which provides strategies for actual control after inverse kinematics solving. Currently, an increasingly number of intelligent optimization algorithms is applied to inverse kinematics solving of the variable topology tetrahedral robot system.

Because there is a strong fitting capability for the neural network in solving any complex problems concerning nonlinear mapping, the boundary constraint RBF (BVRBF) is used in the Thesis to construct the model of the variable topology tetrahedral robot, achieving effective improvement of model accuracy.

## II. RELATIONSHIP BETWEEN THE KINETIC MODEL AND CONSTRAINS

The Lagrange method is used to establish a dynamic simplified model of the variable topology tetrahedral robot, where the first joint is created as the joint of the variable topology tetrahedral robot, and the second and third joints are set as driving joints. The simplified robot model of the variable topology tetrahedral robot with plane three connecting rods are shown in fig.1 where $M_i$ is mass of connecting rod $i$, $E_i$ is the length of connecting rod $i$, $r_i$ is the distance from center of mass of connecting rod $i$ to the former joint, $I_i$ is the rotational inertia of center of mass of connecting rod $i$, $\tau_i$ is driving torque generated by joint $i$, $i=1,2,3$ is included angle between connecting rod $i$ and x-axis, and $\theta_2$ and $\theta_3$ are included angles between adjacent connecting rods.

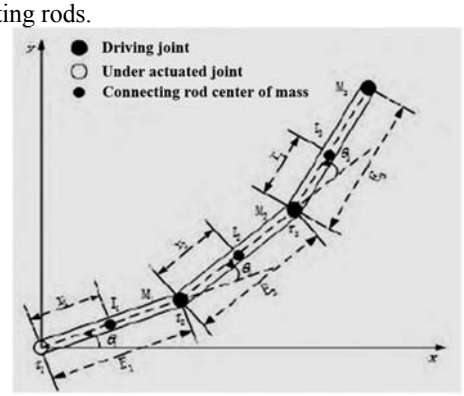


Figure 1. Simplified model of PAA variable topology tetrahedral robot with plane three connecting rods

If $\theta=[\theta_1,\theta_2,\theta_3]$ where $\dot{\theta}$ is the angular speed of system joint angle, the general form of the lagrange equation is:

$$\frac{d}{dt}\left(\frac{\partial L(\theta,\dot{\theta})}{\partial \dot{\theta}_i}\right)-\frac{\partial L(\theta,\dot{\theta})}{\partial \theta_i}=T_i \tag{1}$$

That is, lagrangian $L(\theta,\dot{\theta})$ is difference between kinetic energy and potential energy of the system, that is:

$$L(\theta,\dot{\theta})=T(\theta,\dot{\theta})-G(\theta,\dot{\theta}) \tag{2}$$

The variable topology tetrahedral robot system with plane three connecting rods is a plane motion system, so system's $G(\theta,\dot{\theta})$ is constant to be zero. Each rod's motion $T_i$ and energy $T_2$ for the rod's rotation around its center of mass constitute center of mass motion. The system's total kinetic energy is:

$$T(\theta,\dot{\theta})=T_1+T_2 \tag{3}$$

For each rod, the following can be calculated:

$$T_i=\frac{1}{2}I_i\dot{\theta}^2+\frac{1}{2}M_iV_i^2, i=1,2,3 \tag{4}$$

$V_i$ is the movement velocity of center of mass, which can be derived from sum of derivative squares in the center-of-mass coordinate of connecting rod $i$ vs time. Derivatives and partial derivatives corresponding to each rod are substituted into the lagrange equation, and then the dynamics description equation is derived in respect of the plane variable topology tetrahedral robot system.

$$D(\theta)\ddot{\theta}+F(\theta,\dot{\theta})=\tau \tag{5}$$

Where, $D(\theta)$ is the system's inertial matrix with positive definiteness and symmetry, $\ddot{\theta}$ is the accelerated speed of angle of the system, and $F(\theta,\dot{\theta})=[F_1,F_2,F_3]^T$ is the combined matrix of coriolis force with centrifugal force. Because the first joint is the passive joint, so $\tau_1=0$ and the driving force torque matrix $\tau=[0,\tau_2,\tau_3]^T$ as well as:

$$D=\begin{bmatrix} D_{11} & D_{12} & D_{13} \\ D_{21} & D_{22} & D_{23} \\ D_{31} & D_{32} & D_{33} \end{bmatrix} \tag{6}$$

Where,

$D_{11}=d_1+d_2+d_4+2d_3\cos(\theta_2)+2d_6\cos(\theta_3)+2d_5\cos(\theta_2+\theta_3)$

$D_{12}=d_2+d_4+d_3\cos(\theta_2)+2d_6\cos(\theta_3)+d_5\cos(\theta_2+\theta_3)$ ,

$D_{23}=d_4+d_6\cos(\theta_3)$

$D_{13}=d_4+d_6\cos(\theta_3)+d_5\cos(\theta_2+\theta_3)$ ,

$D_{22}=d_2+d_4+2d_6\cos(\theta_3)$ , $D_{33}=d_4$

$D_{21}=D_{12}$ , $D_{31}=D_{13}$ ,

$F_3=d_5\dot{\theta}_1^2\sin(\theta_2+\theta_3)+d_6(\dot{\theta}_1+\ddot{\theta}_2)^2\sin(\theta_3)$

$F_1=-d_5(2\dot{\theta}_1+\dot{\theta}_2+\dot{\theta}j_3)(\dot{\theta}_2+\dot{\theta}_3)\sin(\theta_2+\theta_3)-d_6(2\dot{\theta}_1+2\dot{\theta}_2+\dot{\theta}_3)\dot{\theta}_3\sin(\theta_3)-d_3($

$F_2=d_3\dot{\theta}_1^2\sin(\theta_2)-d_6(2\dot{\theta}_1+2\dot{\theta}_2+\dot{\theta}j_3)\dot{\theta}_3\sin(\theta_3)+d_5\dot{\theta}_1^2\sin(\theta_2+\theta_3)$

From equation relation of dynamics formula (5), the state constraint equation of the variable topology tetrahedral robot's joint and driving joint is:

$$D_{11}\ddot{\theta}_1+D_{12}\ddot{\theta}_2+D_{13}\ddot{\theta}_3+F_1=0 \tag{7}$$

## III. BVRBF NEURAL NETWORK TOPOLOGY STRUCTURE

The variable topology tetrahedral robot is a nonlinear function. To measure constraint conditions for boundary values of the variable topology tetrahedral robot at this time, the BVRBF neural network and the traditional RBF neural network are adopted to produce a better nonlinear dynamic modeling effect for the variable topology tetrahedral robot.

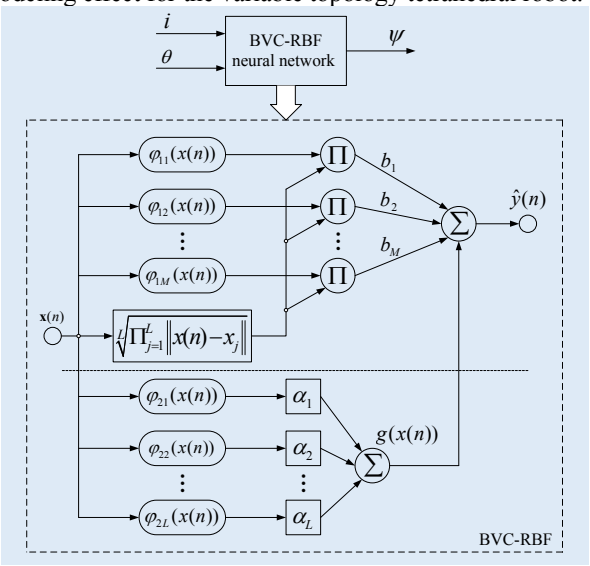


Figure 2. BVRBF neural network topology model

Fig.2 is BVRBF neural network topology structure. From the figure, this network is a nonlinear system with double inputs and single output. SRM phase angle $i$ and angle $\theta$ at the mechanical arm position are selected as input variables of the neural network, while the variable topology tetrahedral robot's mechanical arm position serves as the only output variable of the network system.

SRM flux linkage values computed in real time, and two input variables and one output variable constitute the corresponding data combination. Therefore, the input of defined BVRBF neural network is:

$$\mathbf{x}(n)=[i(n),\theta(n)]^T \tag{8}$$

The output of defined network:

$$\hat{\mathbf{y}}(n) = \psi(n) \tag{9}$$

If the training dataset *D*N including N input-output datasets is $\{x(n),y(n)\}$, the desired output response is:

$$y(n) = f(\mathbf{x}(n), b) + e(n) \tag{10}$$

Where, modeling function *f* is the RBF neural network that achieves $R2 \rightarrow R1$; *b* is the connection weight value of vector; $e(n)$ is the residual error.

Meanwhile, the model strictly meets the constraint condition for boundary values:

$$f(\mathbf{x}_j) = d_j, j = 1,...,L \tag{11}$$

Where, $\boldsymbol{X}\mathrm{j} \in R2$, $d\mathrm{j} \in R1$. The constraint condition for boundary values gives some priori knowledge, which will help improve modeling accuracy.

As shown in fig.3, the modeling function *f*: $R2 \rightarrow R1$ is described by the BVRBF neural network.

$$\hat{y}(n) = \sum_{k=1}^{M} p_k(x(n)) b_k + g(x(n)) \tag{12}$$

Where: $n$=1, 2, …, $N$; $k$=1, 2,…, $M$.

The penalty function $g(x(n))$ is defined by the following equation:

$$\begin{aligned} g(x(n)) &= \sum_{j=1}^{L} \alpha_j \varphi_{2j}(x(n)) \\ &= \sum_{j=1}^{L} \alpha_j \exp(-\frac{\left\| \mathbf{x}(n) - x_j \right\|^2}{\sigma_2^2}) \end{aligned} \tag{13}$$

Where: $\sigma 2$ is the positive scalar and $\alpha \mathrm{j}$ is a set of a series of weights. Hence,

$$\boldsymbol{\alpha} = \mathbf{G}^{-1}\mathbf{d} \tag{14}$$

If $z(n)=y(n)-g(x(n))$ is defined and equation (8) is substituted into equation (6), $z(n)$ can be expressed by

$$z(n) = \sum_{k=1}^{M} p_k(x(n)) b_k + e(n) \tag{15}$$

From equation (15), the problem now is translated into nonlinear modeling of the traditional RBF neural network. The specific nonlinear modeling of the BVRBF neural network can be divided into the following two parts:

1) Solve the constraint condition equation of boundary values to obtain the penalty function $g(x(n))$;

2) Use the universal training algorithm to train the traditional RBF neural network.

## IV. MODELING BASED ON FLUX LINKAGE CHARACTERISTIC OF BVRBF

The orthogonal least square method is adopted in the Thesis for training of the BVRBF neural network as a positive or inverse system algorithm for reduction of the size of RBF neural network. Equation (15) can be written in the form of matrix.

$$\mathbf{Z} = \mathbf{P}\mathbf{B} + \mathbf{E} \tag{16}$$

Definition

$$\begin{cases} \mathbf{Z} = [z(1), z(2), ..., z(N)]^T \\ \mathbf{B} = [b_1, b_2, ..., b_M]^T \\ \mathbf{E} = [e(1), e(2), ..., e(N)]^T \end{cases} \tag{17}$$

The invertible matrix **P** can broken down into orthogonal vectors below by Gram Schmidt Othogonalization (GSO)

$$\begin{aligned} \mathbf{P} &= \mathbf{W}\mathbf{A} = [\mathbf{w}_1, \mathbf{w}_2, ..., \mathbf{w}_M] \\ &\begin{pmatrix} 1 & a_{12} & \cdots & a_{1M} \\ 0 & 1 & \cdots & \cdots \\ \cdots & \cdots & \cdots & a_{M-1,M} \\ 0 & 0 & \cdots & 1 \end{pmatrix} \end{aligned} \tag{18}$$

Where, $\mathbf{A} \in \Re^{M \times M}$ is the upper triangular matrix, $\mathbf{W} \in \Re^{N \times M}$, and element $\mathbf{w}_i$ is the mutually orthogonal vector. Hence,

$$\mathbf{W}^T\mathbf{W} = \mathbf{\Lambda} = diag(\lambda_1, \lambda_2, ..., \lambda_M) \tag{19}$$

Where, $\lambda i$ is the element of diagonal matrix, and when $j \neq l$, the condition of $\boldsymbol{W}j\mathrm{T}\boldsymbol{W}l=0$ is satisfied.

Assuming $\mathbf{\Gamma} = \mathbf{A}\mathbf{B}$, the following can be derived if equation (15) is substituted into equation (12) at this time.

$$\mathbf{Z} = \mathbf{W}\mathbf{\Gamma} + \mathbf{E} \tag{20}$$

The orthogonal least square method is adopted to decompose equation (16).

$$\hat{\mathbf{\Gamma}} = \mathbf{\Lambda}^{-1}\mathbf{W}^T\mathbf{Z} \tag{21}$$

Therefore, from equations (20) and (21), availability of the connection weight matrix is guaranteed. Considering that

the orthogonal least square (OLS) algorithm guarantees the mutual orthogonality of matrix $\mathbf{W\Gamma}$ and matrix $\mathbf{E}$ in equation (21), so

$$\begin{aligned}\mathbf{Z}^T\mathbf{Z} &= \mathbf{\Gamma}^T\mathbf{W}^T\mathbf{W\Gamma} + \mathbf{E}^T\mathbf{E} \\ &= \sum_{k=1}^{M}\lambda_k\tau_k^2 + \mathbf{E}^T\mathbf{E}\end{aligned} \tag{22}$$

At this time, the corresponding Error Reduction Ratio (ERR) is determined by number k generalized constant.

$$err_k = \frac{\lambda_k\tau_k^2}{\mathbf{Z}^T\mathbf{Z}} \tag{23}$$

Equation (23) gives an effective method to obtain a generalized constant during the course of positive regression of RBF. During the positive regression of each step of training, sufficient RBF center is selected to maximize ERR value and the training can stop till the regression course in the case of equation (2:4) is satisfied.

$$1-\sum_{k=1}^{M_0} err_k < \varepsilon, 0<\varepsilon<1 \tag{24}$$

## V. EXPERIMENTAL RESULTS AND ANALYSIS

In the simulation experiment, the simulation step size is 0.001s, original angle $\theta(0)=[1.57,0,0]$, and the coordinate of corresponding tail end point position is $(0,3)$, with 200 groups of training samples and 40 groups of testing samples selected. During the course of the training, the Monte Carlo method is used to produce input data in working space which then undergoes normalization processing to make input data within [-1, 1]. The effects on target functions are the same. Randomness is increased to avoid falling into the local optimum to the greatest extent. When particle swarms converge, sample data is used for simulation test. Target location values in the test samples are input into the neural network, calculated joint values are derived. The sample error range derived by the calculated joint values minus actual joint values of the test samples is [-0.0391, 0.0383]. Fig.3 is the error curve for test samples of the three joints. From the figure, the angle error of the proposed algorithm in the Thesis is less than $0.080^0$.

Integer programming particle swarm optimization (algorithm 1), BP calibrated neural network (algorithm 2) and proposed algorithm in the Thesis (algorithm 3) are respectively used to solve based on the same sample data. The comparative result of accuracy error is presented in table 1.

From table 1, the proposed algorithm has the highest accuracy of network solution, meeting the requirement for high accuracy in the practical application. Comparison of rate of convergence is shown in fig.4 from which the integer programming particle swarm optimization has the slowest rate of convergence. Because such operations as variation and selection are required for the neural network by particle swarm optimization, the training time is longer than BP calibration. The proposed algorithm overcomes the defect of slow rate of convergence to some extent and the effectiveness of the proposed algorithm is verified.

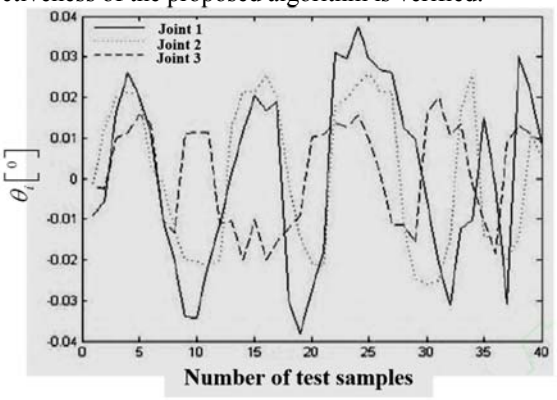


Figure 3. Error curve of test samples of joints

TABLE 1. COMPARISON OF OPERATING RESULTS

| Algorithm | Minimum error [o] | Maximum error [o] | Average error [o] |
|---|---|---|---|
| Integer programming particle swarm optimization | 0.1056 | 0.2156 | 0.1985 |
| BP calibrated neural network | 0.0562 | 0.1264 | 0.0968 |
| Proposed algorithm | 0.0126 | 0.0328 | 0.0285 |

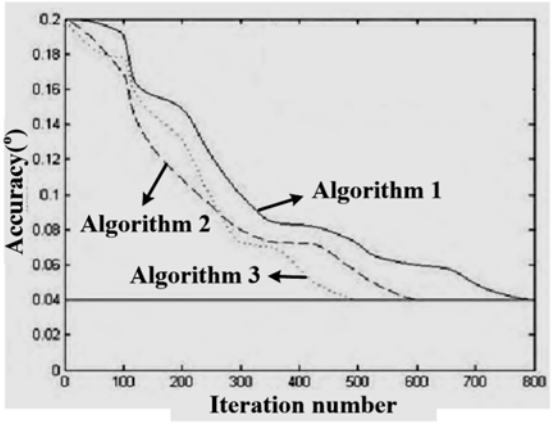


Figure 4. Comparison of rate of convergence

## VI. CONCLUSIONS

A method for construction of the model of the variable topology tetrahedral robot based on the boundary constraint RBF is proposed in the Thesis. Dynamics equations and their integral characteristics are analyzed. Constraint conditions for boundary values of solution are used to obtain the penalty function, while the least square method is adopted to train the traditional RBF neural network to realize construction of the model of the variable topology tetrahedral robot.

Efficiency of the proposed method is verified by the experimental results.

## ACKNOWLEDGMENTS

Sponsored by the Shanghai Academy of Space Technology(SAST201318).

## REFERENCES

[1] Miclosina C O, Cojocaru V, Korka Z I. Dynamic Simulation of a Parallel Topology Robot Operation[J]. Applied Mechanics & Materials, 2015, 762:107-112.

[2] Chen H, Tian F F, Cao G Z, et al. Mechanism design and dynamic simulation of high maneuverable mobile platform for wall-climbing robot[C]// Information Science and Technology (ICIST), 2014 4th IEEE International Conference on. IEEE, 2014:817-820.

[3] Chen H, Tian F F, Cao G Z, et al. Mechanism design and dynamic simulation of high maneuverable mobile platform for wall-climbing robot[C]// Information Science and Technology (ICIST), 2014 4th IEEE International Conference on. IEEE, 2014:817-820.

[4] Choo Y, Casarella M J. A Survey of Analytical Methods for Dynamic Simulation of Cable-Body Systems.[J]. Journal of Hydronautics, 2015, 7(4):137-144.

[5] Jinyu Hu and Zhiwei Gao. Distinction immune genes of hepatitis-induced heptatocellular carcinoma[J]. Bioinformatics, 2012, 28(24): 3191-3194.

[6] Jiang, D., Ying, X., Han, Y., & Lv, Z. (2016). Collaborative multi-hop routing in cognitive wireless networks. Wireless personal communications, 86(2), 901-923.

[7] Lv, Z., Tek, A., Da Silva, F., Empereur-Mot, C., Chavent, M., & Baaden, M. (2013). Game on, science-how video game technology may help biologists tackle visualization challenges. PloS one, 8(3), e57990.

[8] Jiang, D., Xu, Z., & Lv, Z. (2015). A multicast delivery approach with minimum energy consumption for wireless multi-hop networks. Telecommunication systems, 1-12.

[9] Lv, Z., Chirivella, J., & Gagliardo, P. (2016). Bigdata Oriented Multimedia Mobile Health Applications. Journal of medical systems, 40(5), 1-10.

[10] Wang X, Wang X, Zhang Z, et al. Motion Planning of Kinematically Redundant 12-tetrahedral Rolling Robot[J]. International Journal of Advanced Robotic Systems, 2016, 13.

[11] Allotta B, Costanzi R, Meli E, et al. Cooperative localization of a team of AUVs by a tetrahedral configuration[J]. Robotics & Autonomous Systems, 2014, 62(8):1228-1237.

[12] Yang T, Yang T, Yin H, et al. Interaction modeling and simulation of a flexible needle insertion into soft tissues[C]// Isr/robotik 2014;, International Symposium on Robotics; Proceedings of. VDE, 2014:1 - 6.

[13] Müller-Fischer M. Hierarchical position-based dynamics: The Eurographics Association, US8996337[P]. 2015.

[14] Li W, Chen R, Tan Z. Efficient Sequential Monte Carlo with Multiple Proposals and Control Variates[J]. Journal of the American Statistical Association, 2015:00-00.

[15] Liu F, Hager W W, Rao A V. Adaptive Mesh Refinement Method for Optimal Control Using Nonsmoothness Detection and Mesh Size Reduction[J]. Journal of the Franklin Institute, 2015, 47(10).

[16] Sun Z, Helmke U, Anderson B. Rigid formation shape control in higher dimensions: an invariance principle and open problems[J]. 2015.

[17] Chen S C, Huang C H, Yang C S, et al. Crystal structure of Deinococcus radiodurans RecQ helicase catalytic core domain: the interdomain flexibility.[J]. Biomed Research International, 2014, 2014:342725-342725.

[18] Yang, J., Lin, Y., Gao, Z., Lv, Z., Wei, W., & Song, H. (2015). Quality index for stereoscopic images by separately evaluating adding and subtracting. PloS one, 10(12), e0145800.

[19] Lv, Z., & Li, X. (2015, November). Virtual Reality Assistant Technology for Learning Primary Geography. In International Conference on Web-Based Learning (pp. 31-40). Springer International Publishing.

[20] Feng, L., Lv, Z., Guo, G., & Song, H. (2016). Pheromone based alternative route planning. Digital Communications and Networks, 2(3), 151-158.

.